
Accelerating Masked Image Generation by Learning Latent Controlled Dynamics

Kaiwen Zhu^{*12} Quansheng Zeng²³⁴ Yuandong Pu¹² Shuo Cao²⁵ Xiaohui Li¹² Yi Xin²³⁶ Qi Qin²⁷
Jiayang Li²⁸ Yu Qiao²³ Jinjin Gu⁹ Yihao Liu²

Abstract

Masked Image Generation Models (MIGMs) have achieved great success, yet their efficiency is hampered by the multiple steps of bi-directional attention. In fact, there exists notable redundancy in their computation: when sampling discrete tokens, the rich semantics contained in the continuous features are lost. Some existing works attempt to cache the features to approximate future features. However, they exhibit considerable approximation error under aggressive acceleration rates. We attribute this to their limited expressivity and the failure to account for sampling information. To fill this gap, we propose to learn a lightweight model that incorporates both previous features and sampled tokens, and regresses the average velocity field of feature evolution. The model has moderate complexity that suffices to capture the subtle dynamics while keeping lightweight compared to the original base model. We apply our method, *MIGM-Shortcut*, to two representative MIGM architectures and tasks. In particular, on the state-of-the-art Lumina-DiMOO, it achieves over $4\times$ acceleration of text-to-image generation while maintaining quality, significantly pushing the Pareto frontier of masked image generation. The code and model weights are available [here](#).

1. Introduction

Masked Image Generation Models (MIGMs) present a prominent paradigm for visual generation. They typically

^{*}Work done during internship at Shanghai Artificial Intelligence Laboratory ¹Shanghai Jiao Tong University, Shanghai, China ²Shanghai Artificial Intelligence Laboratory, Shanghai, China ³Shanghai Innovation Institute, Shanghai, China ⁴Nankai University, Tianjin, China ⁵University of Science and Technology of China, Hefei, China ⁶Nanjing University, Nanjing, China ⁷The University of Sydney, Sydney, Australia ⁸Peking University, Beijing, China ⁹INSAIT, Sofia, Bulgaria. Correspondence to: Yihao Liu <liuyihao@pjlab.org.cn>.

model the image as a sequence of discrete tokens, and predict them from a “mask” state progressively to generate an image. When scaled up, they have achieved strong performance that is comparable to the cutting-edge continuous diffusion models (Xie et al., 2023; You et al., 2025). Moreover, their formulation can be seamlessly unified with the generation of other modalities. Recognizing this, the recently emerging multi-modal masked diffusion models have incorporated MIGMs’ paradigm to exhibit versatile generation capabilities (Yang et al., 2025; Xin et al., 2025).

As MIGMs are increasingly integrated into large-scale foundation models, an imperative demand is to improve their efficiency. One way is to reduce the number of generation steps. However, implementing this is hindered by the multi-modality problem (Gu et al., 2018), that is, standard MIGMs struggle to model the joint distribution of multiple tokens in a single step. Another way is to reduce the cost of each step. Inspired by the KV-cache mechanism in auto-regressive models, many works propose to reuse the features in previous steps considering that the token features often remain stable (Liu et al., 2025d;e; Xin et al., 2025). Despite some success, they are mostly based on intuitively handcrafted rules and the acceleration effect is still limited.

The caching-based methods are also well-developed for continuous diffusion models, and a trend is to shift from reusing to predicting (Liu et al., 2025b). Some works view the features across steps as an evolving trajectory. They argue that this trajectory is smooth and thus can be predicted by simple computation. For example, TaylorSeer (Liu et al., 2025c) and HiCache (Feng et al., 2025) predict the next feature by polynomial expansions, assuming the feature trajectory is sufficiently well-behaved.

Along this research line, we investigate whether the smoothness also holds true for MIGMs. Using Lumina-DiMOO (Xin et al., 2025) to generate samples, we investigate the features in the last layer of the model¹. We compute the temporal self-similarity and visualize the trajectory using t-SNE (van der Maaten & Hinton, 2008). An example

¹In the rest of the paper, the term “feature” always refers to the last layer’s feature. For the rationale please refer to Appendix A.

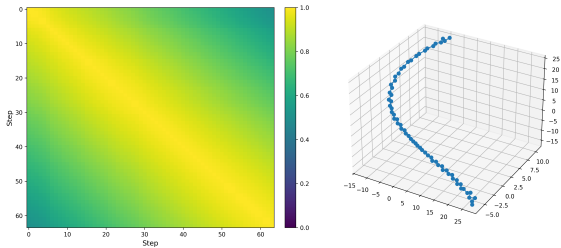
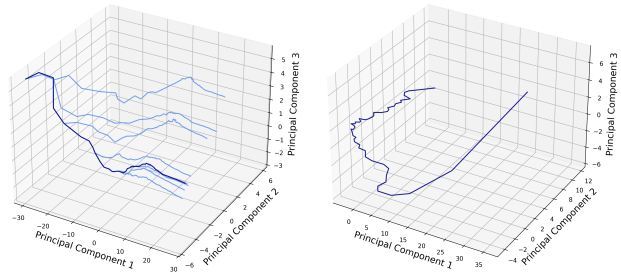


Figure 1. Visualization of trajectory smoothness. A point in the trajectory is the feature averaged over all tokens in a step. Left: heatmap of pairwise cosine similarity; Right: t-SNE visualization.

is shown in Fig. 1. The features in consecutive steps are extremely similar, and the visualized trajectory exhibits a regular pattern. This suggests that as the model tries to learn the trajectory of token generation, it has also learned a latent trajectory in its internal feature space that underlies that generation process. This latent space may be more well-structured and thus more conducive to modelling.

In spite of the similar observation, we cannot directly apply the existing methods for continuous diffusion on MIGMs. These methods require that the feature dynamics are self-contained, that is, the entire trajectory is uniquely determined by its own history, receiving no exogenous inputs. This is valid under the ODE sampling of continuous diffusion models. However, it is not the case for MIGMs. As the starting point is always a fully masked sequence without randomness, the diversity must rely on the sampling in the generation process. The randomness in sampling tokens directs the trajectory to various samples. As illustrated in Fig. 2a, starting from the same point, if we change the random seed at an intermediate stage of generation, then the trajectory will fork, generating diverse samples. As a result, it is ill-posed to predict future features from the past features alone, which is what existing methods for continuous diffusion do. We must model the dynamics controlled by the observed sampling results (Kidger et al., 2020).

This work seeks to tackle this challenge. Accounting for the sampled tokens greatly increases the complexity of modelling, so the simple training-free methods (Liu et al., 2025c; Feng et al., 2025; Zheng et al., 2025b) are not optimal. We propose to learn this latent controlled dynamics with a neural network. Based on the observation that the trajectory is smooth to some extent, this network may not require particularly high complexity. Therefore, we choose to use a lightweight model to learn the feature dynamics. The model takes as input the feature and sampled tokens in the previous step, and predicts the direction to the next feature. Once the feature dynamics are learned, at inference time we can replace the original heavy base model with this lightweight model in many steps, saving computation and accelerating generation. We term this model as a *shortcut*, since it takes the smoother path in the latent feature space.



(a) MIGM’s feature trajectories. (b) Diffusion’s feature trajectories using ODE sampling.

Figure 2. PCA visualization of feature trajectories generated with the same prompt and initial random seed. (a) Using a MIGM, we first generate a trajectory (the dark one) and then change the random seed at intermediate steps to generate more samples (the light ones). The randomness in sampling tokens greatly affects the generation process. (b) In contrast, for continuous diffusion with ODE sampling, trajectories generated from the same starting point are always the same, without randomness at intermediate steps.

We instantiate our method, MIGM-Shortcut, on two representative models, the seminal work MaskGIT (Chang et al., 2022) and the recent state-of-the-art model Lumina-DiMOO (Xin et al., 2025). Extensive experiments validate the rationale and effectiveness of our method. For example, we achieve over $4\times$ speedup for Lumina-DiMOO with negligible performance drop on the text-to-image task. MIGM-Shortcut not only yields practical acceleration benefits, but also brings up a perspective of learning latent dynamics, which we demonstrate to be simple yet effective. Beyond the acceleration effects, we hope MIGM-Shortcut could provide more insights into masked generative models and advance the development of this field.

2. Related Work

2.1. Masked Image Generation

Discrete image generation is initially dominated by the autoregressive models, which predict the next pixel or vector-quantized token following a specific order, usually as raster scan (van den Oord et al., 2016; Parmar et al., 2018; Ramesh et al., 2021; Esser et al., 2021). They suffer from two limitations. First, the number of network evaluations equals the number of pixels or tokens, requiring prohibitive computation cost. Second, the causal attention restricts the model from attending to future tokens and thus limits the information interaction, but it is hard to predefine an appropriate generation order that could alleviate this limitation. In view of this, MaskGIT (Chang et al., 2022) proposes the masked image generation paradigm inspired by BERT (Devlin et al., 2019). It takes as input a randomly masked token sequence and predicts multiple tokens within a single network evaluation, thereby overcoming inefficiency and the rigid gen-

eration order. Moreover, courtesy of the flexibility in the conditioning masked positions, MIGMs can be applied to image editing without fine-tuning (Chang et al., 2022; 2023). It is also revealed that masked image modeling could help in representation learning (He et al., 2022; Li et al., 2023; Xie et al., 2022; 2023). To further boost the performance of MIGMs, many works present improvements on various components, including the sampler (Besnier et al., 2025), mask schedule (Shao et al., 2024), hyper-parameter optimization (Ni et al., 2024a), and model architecture (Ni et al., 2024b; Bai et al., 2025), achieving performance comparable to the state-of-the-art models in image generation (You et al., 2025). It is interesting to note that MIGMs can be connected with masked diffusion, which performs the diffusion process on categorical data (Austin et al., 2021; You et al., 2025). This paradigm enables the unification of processing different modalities. Recognizing this, MMaDA (Yang et al., 2025) and Lumina-DiMOO (Xin et al., 2025) formulate various tasks as modeling sequences interleaved with text and images, exhibiting versatile capabilities in multi-modal generation.

2.2. Image Generation Acceleration

High-quality image generation often requires multiple steps, incurring significant latency. To alleviate this, many works propose to reduce the number of steps, achieving few-step or even one-step generation for continuous diffusion models (Salimans & Ho, 2022; Lu et al., 2022; Song et al., 2023; Yin et al., 2024; Frans et al., 2025; Geng et al., 2025). There are also a few works making such efforts for discrete diffusion models (Zhu et al., 2025; Kim et al., 2025). Despite success to some extent, they struggle to sufficiently address the multi-modality problem (Gu et al., 2018). Other works seek to reduce the cost of each generation step. Typical approaches include pruning (Fang et al., 2023), quantization (Shang et al., 2023), and caching (Liu et al., 2025b). Our work is most closely related to caching-based methods. They observe that the learned token features in consecutive steps are often highly similar, so it is possible to approximate the features using those in previous steps (Ma et al., 2024; Selvaraju et al., 2024; Chen et al., 2025a). To reduce the approximation error, many methods have been developed to adaptively identify reusable features (Chen et al., 2024; Yan et al., 2025; Xin et al., 2025) or improve the refresh schedule (Qiu et al., 2025; Wimbauer et al., 2024; Liu et al., 2025a). Beyond directly replacing target features with cached features, some works perform cheap transformations on them. For example, FoCa (Zheng et al., 2025b), TaylorSeer (Liu et al., 2025c), and HiCache (Feng et al., 2025) treat the feature as a function of time, so future features can be predicted using ODE solvers or polynomial expansions. However, these methods often require the feature to be differentiable with respect to time, which does not hold true for

discrete diffusion. TeaCache (Liu et al., 2025a) and Block Caching (Wimbauer et al., 2024) represent target features as polynomials of cached features and learn the coefficients, as a trick to refine the cache. In contrast to these works, our method focuses on learning a feasible feature dynamics model with moderate complexity, and can be readily applied to various existing well-trained base models.

3. Method

We first define the notations and formulate the shortcut model (Sec. 3.1). Next, we provide intuition and empirical evidence for our assumption (Sec. 3.2). Then we outline the concrete implementation of the neural network (Sec. 3.3). Finally, we describe the training (Sec. 3.4) and usage (Sec. 3.5) of the model.

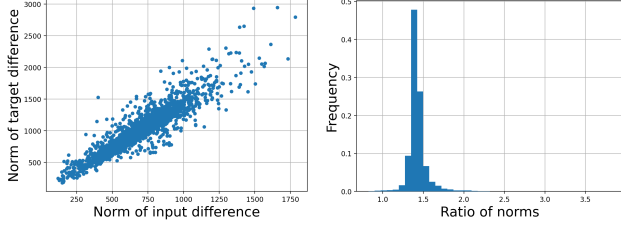
3.1. Formulation

Preliminary and Notation. We adopt the typical framework of discrete masked image generation (Chang et al., 2022; Li et al., 2023; Bai et al., 2025). Let \mathcal{V} denote the vocabulary produced by the discrete tokenizer. A special token $[\text{mask}]$ is introduced to form the augmented vocabulary $\tilde{\mathcal{V}} = \mathcal{V} \cup \{[\text{mask}]\}$. The generation process is represented by $\{\mathbf{x}_t\}_{t \in [0,1]}$, where $\mathbf{x}_t \in \tilde{\mathcal{V}}^L$ and L is the number of tokens in the image. Starting from the fully masked $\mathbf{x}_0 = ([\text{mask}], [\text{mask}], \dots, [\text{mask}])$, the number of masked tokens progressively reduces, leading to the fully unmasked image $\mathbf{x}_1 \in \mathcal{V}^L$. Formally, define a scheduler $\gamma : [0, 1] \rightarrow [0, 1]$ so that $\gamma(0) = 1, \gamma(1) = 0$, and γ monotonically decreases. $\gamma(t)$ represents the mask ratio at time t . In practice, the generation process is discretized into N steps $\{t_i = i/N\}_{i=0}^N$. At step i , the unmasking model M predicts the distribution over \mathcal{V} of each token $\mathbf{p}_{t_i} = M(\mathbf{x}_{t_{i-1}})$. Sampling from \mathbf{p}_{t_i} yields $\hat{\mathbf{x}} \in \mathcal{V}^L$. With some strategy, $\lceil L \cdot \gamma(t_{i-1}) \rceil - \lceil L \cdot \gamma(t_i) \rceil$ masked positions in $\mathbf{x}_{t_{i-1}}$ are selected and filled with the corresponding tokens in $\hat{\mathbf{x}}$, obtaining \mathbf{x}_{t_i} . A typical selection strategy is the confidence-based sampler (Chang et al., 2022). Denote this sampling process by $\mathbf{x}_{t_i} \sim K(\cdot | \mathbf{x}_{t_{i-1}}, \mathbf{p}_{t_i}, \gamma, t_{i-1}, t_i)$. The above procedure repeats for $i = 1, 2, \dots, N$ to generate the final sample \mathbf{x}_1 .

Model. Let $\mathbf{f}_{t_i} = M_f(\mathbf{x}_{t_{i-1}}) \in \mathbb{R}^{L \times D}$ denote the last hidden state of the unmasking model M , that is, $\mathbf{p}_{t_i} = \text{softmax}(H(\mathbf{f}_{t_i}))$, where H is the classification head. We view $\{\mathbf{f}_{t_i}\}_{i=1}^N$ as a latent controlled trajectory that underlies the generation process, and propose to capture its dynamics by learning. Treating $\{\mathbf{x}_t\}$ as the observation and $\{\mathbf{f}_t\}$ as the state, we reformulate the generation process as a state-space model:

State transition

$$\mathbf{f}_{t_{i+1}} = \mathbf{f}_{t_i} + S_\theta(\mathbf{f}_{t_i}, \mathbf{x}_{t_i}, t_i) + \epsilon, \quad (1)$$



(a) Scatter plot of the norms of the input/target difference. (b) Frequency histogram of the ratio of the two norms.

Figure 3. Observation of local Lipschitz behavior. Consider the map (3). For neighboring points along trajectories, we compute the norms of the target and input differences. The ratio of the two norms concentrates around a moderate constant.

Observation

$$\mathbf{x}_{t_{i+1}} \sim K(\cdot | \mathbf{x}_{t_i}, \text{softmax}(H(\mathbf{f}_{t_{i+1}})), \gamma, t_i, t_{i+1}). \quad (2)$$

Here, S_θ is a lightweight neural network with learnable parameter θ , and ϵ is the error term that follows a normal distribution with zero mean. We call S_θ the *shortcut* model, highlighting that it bypasses the cumbersome base model M by taking a shortcut from \mathbf{f}_{t_i} that directly leads to $\mathbf{f}_{t_{i+1}}$.

3.2. Rationale

In this section, we discuss why the map²

$$(\mathbf{f}_{t_i}, \mathbf{x}_{t_i}) \mapsto \mathbf{f}_{t_{i+1}} - \mathbf{f}_{t_i} \quad (3)$$

in the shortcut model S_θ could have far lower complexity than the map $\mathbf{x}_{t_i} \mapsto \mathbf{f}_{t_{i+1}}$ in the original base model M . As Fig. 1 shows, \mathbf{f}_{t_i} and $\mathbf{f}_{t_{i+1}}$ are very close, with a cosine similarity usually larger than 0.95. Note that such high similarity is not just because they share the same space. In fact, in the sampling process (2), many tokens collapse into [mask], discarding the rich information contained in the continuous features. This information loss is irreversible. As a result, to obtain $\mathbf{f}_{t_{i+1}}$ solely from \mathbf{x}_{t_i} , the base model M must compute the features of masked tokens from scratch, which is already largely contained in \mathbf{f}_{t_i} . Therefore, taking \mathbf{f}_{t_i} as input to supplement information will significantly alleviate the computational burden. However, using \mathbf{f}_{t_i} alone is insufficient either, as the sampling process (2) itself also contains crucial information. The sampled \mathbf{x}_{t_i} directly points out the direction from $\mathbf{f}_{t_i} = M_f(\mathbf{x}_{t_{i-1}})$ to $\mathbf{f}_{t_{i+1}} = M_f(\mathbf{x}_{t_i})$. Without \mathbf{x}_{t_i} , the map would be stochastic, hence when trained in a supervised learning manner, the model inevitably outputs blurry expectations (Isola et al., 2017). Collectively, combined with the residual connection (He et al., 2016) in Eq. (1), the map (3) describes how the latent

²The time t_i is omitted in the input for simplicity. In fact, it is more like an auxiliary term and can be implicitly captured by \mathbf{f}_{t_i} (Zheng et al., 2025a).

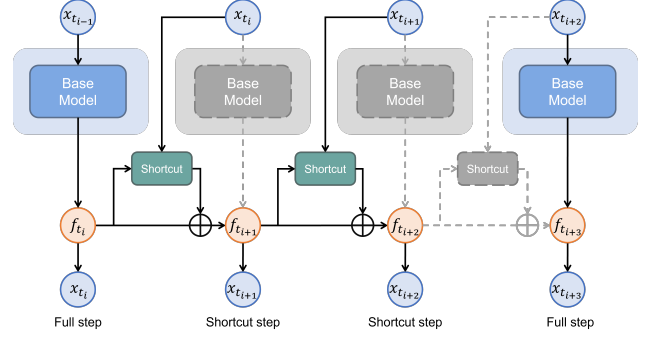


Figure 4. Inference workflow of MIGM-Shortcut. Colored blocks and solid lines represent activated computation, while gray blocks and dash lines represent suppressed computation. At a full step, the inference is the same as the vanilla procedure, taking $\mathbf{x}_{t_{i-1}}$ as input to compute \mathbf{f}_{t_i} using the base model. At a shortcut step, the shortcut model takes $\mathbf{x}_{t_{i-1}}$ and $\mathbf{f}_{t_{i-1}}$ as input to compute \mathbf{f}_{t_i} , leaving the heavy base model skipped.

state evolves driven by a newly sampled observation. In summary, the computation of this map is self-contained and efficient, thanks to the smoothness of the latent dynamics.

To support the simplicity of the map (3), we inspect the local regularity on observed data. We collect 100 trajectories $\{(\mathbf{x}_{t_i}^{(k)}, \mathbf{f}_{t_i}^{(k)}), i = 1, \dots, T\}_{k=1}^{100}$ using Lumina-DiMOO (Xin et al., 2025). Let $\mathbf{u}_i^{(k)}$ denote the concatenation of $E(\mathbf{x}_{t_i}^{(k)})$ and $\mathbf{f}_{t_i}^{(k)}$, where E is the token embedding, and let $\Delta_i^{(k)}$ denote $\mathbf{f}_{t_{i+1}}^{(k)} - \mathbf{f}_{t_i}^{(k)}$. That is, $\mathbf{u}_i^{(k)}$ and $\Delta_i^{(k)}$ represent the input and target of map (3), respectively. We compute the Frobenius norm of their finite differences $\|\mathbf{u}_{i+1}^{(k)} - \mathbf{u}_i^{(k)}\|_F$ and $\|\Delta_{i+1}^{(k)} - \Delta_i^{(k)}\|_F$, and present the scatter plot and frequency histogram of their ratio in Fig. 3. It is observed that the points $(\|\mathbf{u}_{i+1}^{(k)} - \mathbf{u}_i^{(k)}\|_F, \|\Delta_{i+1}^{(k)} - \Delta_i^{(k)}\|_F)$ mostly lie close to a straight line passing through the origin; in other words, the ratio $\|\Delta_{i+1}^{(k)} - \Delta_i^{(k)}\|_F / \|\mathbf{u}_{i+1}^{(k)} - \mathbf{u}_i^{(k)}\|_F$ concentrates around a constant. This observation suggests an approximately uniform local Lipschitz behavior rather than highly variable local amplification. Under this assumption, we can anticipate that the model S_θ is not necessarily required to have much high-frequency representational capacity.

3.3. Shortcut Model

The guideline for designing the shortcut model is to be simple and lightweight. The backbone consists of only a cross-attention layer followed by a self-attention layer (Vaswani et al., 2017). The cross attention is responsible for absorbing the information from the sampled tokens, and the self attention could transform the collected information into the evolving direction. In practice, besides the previous feature, what is fed into the model is the tokens newly decoded in the previous step, carrying position embeddings, instead

of the full token sequence. In the cross attention, the key and value are from these tokens. This highlights that the evolution of features is sufficiently driven by the new tokens, and there is also a practical benefit of efficiency. To further save computational cost, we impose a bottleneck on the model. The inputs are projected to a lower-dimensional space by a linear layer, and projected back at the end of the model. This is reasonable based on the assumption that the latent trajectory evolution is driven by a few newly decoded tokens and thus relatively low-rank. In our default setting the bottleneck ratio is 2.

Additionally, we include time as a conditioning input. The time scalar is transformed into sinusoidal embeddings (Ho et al., 2020) and then modulates the features via adaptive layer normalization (Peebles & Xie, 2023). We empirically find that it could accelerate convergence. This may be because the dynamics are prominently time-variant, so the time conditioning helps the model to be aware of the current stage and accordingly steer its prediction (Bai et al., 2025).

3.4. Training

The training of the shortcut model is straightforward. We collect a dataset of $(\mathbf{f}_{t_i}, \mathbf{x}_{t_i}, t_i, \mathbf{f}_{t_{i+1}})$ as training samples, and optimize the Mean Squared Error (MSE) loss

$$\mathbb{E} \left[\left\| \mathbf{f}_{t_{i+1}} - (\mathbf{f}_{t_i} + S_{\theta}(\mathbf{f}_{t_i}, \mathbf{x}_{t_i}, t_i)) \right\|_2^2 \right]. \quad (4)$$

Only the shortcut model’s parameter θ is trainable, and the base model M remains frozen. The form of the objective resembles that in feature distillation (Romero et al., 2015; Zhang et al., 2022). The subtle difference is that the feature to regress is not auxiliary implicit knowledge, but the only explicit target, and the input is not the same as the teacher’s input, but the previous step’s feature derived by our insights for masked generation.

We have also explored more sophisticated training strategies. We tried to supplement the loss with a distribution matching term like Kullback-Leibler divergence as a regularizer. We also tried to expose the shortcut model to its own predictions as input (Zhou et al., 2024; Huang et al., 2025). However, it turns out that the simple MSE loss (4) alone works as well as these modifications. This in turn partially supports our assumption that the dynamics are easy enough to be learned by a simple approach, while complex designs bring marginal improvements. More details are in Appendix B.

3.5. Inference

At inference time, we first compute \mathbf{f}_{t_1} using the base model M from the masked sequence \mathbf{x}_0 , and in subsequent steps, we can replace the heavy $\mathbf{f}_{t_{i+1}} = M_f(\mathbf{x}_{t_i})$ with the light

$$\hat{\mathbf{f}}_{t_{i+1}} = \mathbf{f}_{t_i} + S_{\theta}(\mathbf{f}_{t_i}, \mathbf{x}_{t_i}, t_i).$$

Table 1. Performance of MaskGIT with and without shortcut. The speedup is with respect to 15-step vanilla, which is the recommended setting of Besnier & Chen (2023). The best and second best performances are marked in **bold** and underline, respectively.

Method	Configuration	Latency (ms)↓	Speedup↑	FID↓
Vanilla	8 steps	26.1	1.92×	9.91
	9 steps	29.4	1.70×	8.86
	11 steps	35.9	1.40×	7.90
	13 steps	42.5	1.18×	7.64
	15 steps	50.1	1.00×	7.60
	32 steps	104.6	0.48×	8.08
Shortcut	15 steps, $B = 7$	25.9	1.94×	8.90
	15 steps, $B = 8$	28.8	1.74×	8.16
	32 steps, $B = 8$	33.7	1.49×	7.30
	32 steps, $B = 9$	36.8	1.36×	<u>6.97</u>
	32 steps, $B = 12$	45.9	1.09×	6.84

However, in fact $\hat{\mathbf{f}}_{t_{i+1}}$ does not equal $\mathbf{f}_{t_{i+1}}$ due to the error term in (1) and the optimization error, so continuously applying the shortcut model will cause distribution shift and keep amplifying the error. To suppress error accumulation, we regularly apply the base model to obtain the feature that follows the correct distribution. Specifically, suppose we generate the image in N steps and have a budget to invoke the base model for B times, then at step $1 + \lfloor jN/B \rfloor$, $j = 0, 1, \dots, B - 1$, we invoke the base model to slowly but accurately compute the feature (full step), and at other steps we invoke the shortcut model to approximately but rapidly compute the feature (shortcut step). Fig. 4 provides an overview of this procedure.

4. Experiments

In this section, we validate the soundness of MIGM-Shortcut by extensive experimental results. As a proof of concept, we first apply our method to the seminal MIGM MaskGIT (Chang et al., 2022) to probe the effectiveness (Sec. 4.1). Then we perform experiments on Lumina-DiMOO (Xin et al., 2025), a multi-modal masked diffusion language model that achieves state-of-the-art text-to-image capability. We will show that equipping it with MIGM-Shortcut, the generation can be greatly accelerated while maintaining the image quality (Sec. 4.2). We also ablate key designs of MIGM-Shortcut to further support our motivation (Sec. 4.3). All training and inference are conducted on NVIDIA H200 GPUs.

4.1. Class-to-Image Generation using MaskGIT

The MaskGIT model we use is from Besnier & Chen (2023). Built upon this, we construct MaskGIT-Shortcut with 8.6M parameters, about 1/20 of the base model. The latency of one invocation is reduced by 24×. We use MaskGIT to generate 50,000 images of resolution 512×512 from the class labels of ImageNet (Deng et al., 2009) in 15 steps. We also use classifier-free guidance, so each image contributes

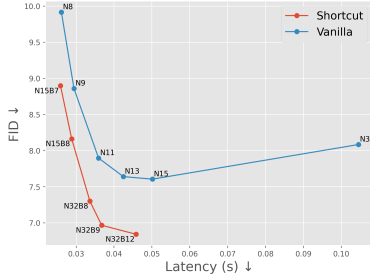


Figure 5. Quality-speed trade-off MaskGIT with and without shortcut. MaskGIT-Shortcut can reach lower FID and faster speed. # steps N and the budget B are marked near the points.

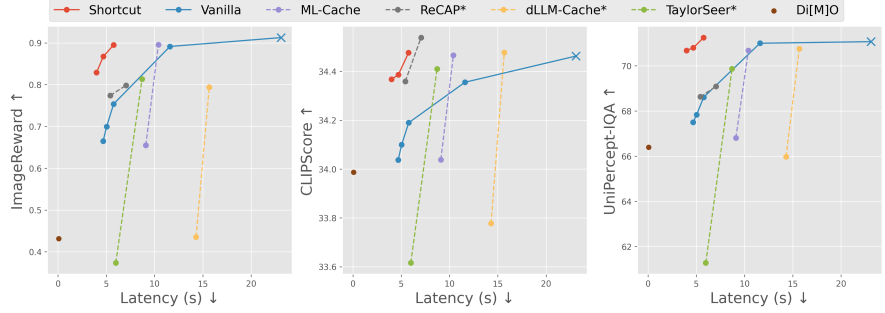


Figure 6. Quality-speed trade-off of different methods accelerating text-to-image generation using Lumina-DiMOO. The point before acceleration is denoted by \times . Dash lines denote existing acceleration methods. DiMOO-Shortcut (red line) significantly pushes the Pareto frontier.



Figure 7. Qualitative comparison of acceleration methods. DiMOO-Shortcut achieves decent quality with $4.9\times$ speedup.

Table 2. Performance of different methods accelerating text-to-image generation using Lumina-DiMOO, along with the one-step model Di[M]O. Apart from the performance before acceleration (Vanilla 64 steps), for each metric the best and second best entries are marked in **bold** and underline, respectively. For ML-Cache, w, r, c represent warmup_ratio, refresh_interval, and cache_ratio in their paper. * denotes methods re-implemented by us on Lumina-DiMOO.

Method	Configuration	Latency (s)↓	Speedup↑	ImageReward↑	CLIPScore↑	UniPercept-IQA↑
Vanilla	64 steps	23.10	1.00×	0.91 (+0.00)	34.46 (+0.00)	71.07 (+0.00)
Few-step Vanilla	32 steps	11.60	1.99×	0.89 (-0.02)	34.35 (-0.11)	<u>71.00</u> (-0.07)
	16 steps	5.77	4.00×	0.75 (-0.16)	34.19 (-0.27)	68.61 (-2.46)
	14 steps	5.04	4.58×	0.70 (-0.21)	34.10 (-0.36)	67.84 (-3.23)
	13 steps	4.68	4.94×	0.67 (-0.24)	34.04 (-0.42)	67.50 (-3.57)
ML-Cache	$(w, r, c) = (0.1, 5, 0.9)$	10.40	2.22×	0.90 (-0.01)	34.47 (+0.01)	70.68 (-0.39)
	$(w, r, c) = (0.0, 5, 0.9)$	9.10	2.54×	0.66 (-0.25)	34.04 (-0.42)	66.81 (-4.26)
ReCAP*	$(u, T, T') = (0, 8, 40)$	7.05	3.28×	0.80 (-0.11)	34.54 (+0.08)	69.09 (-1.98)
	$(u, T, T') = (0, 8, 24)$	5.42	4.26×	0.77 (-0.14)	34.36 (-0.10)	68.63 (-2.44)
dLLM-Cache*	$(K_p, K_r) = (10, 5)$	15.67	1.47×	0.79 (-0.12)	<u>34.48</u> (+0.02)	70.76 (-0.31)
	$(K_p, K_r) = (64, 16)$	14.30	1.62×	0.43 (-0.48)	33.78 (-0.68)	65.98 (-5.09)
TaylorSeer*	$(\mathcal{N}, O) = (4, 2)$	8.71	2.65×	0.81 (-0.10)	34.41 (-0.05)	69.87 (-1.20)
	$(\mathcal{N}, O) = (8, 2)$	5.99	3.86×	0.37 (-0.54)	33.62 (-0.84)	61.28 (-9.79)
Di[M]O		0.07	330.00×	0.43 (-0.48)	33.99 (-0.47)	66.40 (-4.67)
Shortcut	$(N, B) = (64, 14)$	5.76	4.01×	0.90 (-0.01)	<u>34.48</u> (+0.02)	71.25 (+0.18)
	$(N, B) = (64, 11)$	4.70	4.91×	0.87 (-0.04)	34.39 (-0.07)	70.80 (-0.27)
	$(N, B) = (64, 9)$	3.99	5.79×	0.83 (-0.08)	34.37 (-0.09)	70.68 (-0.39)

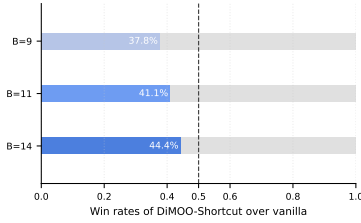


Figure 8. **Win rates of DiMOO-Shortcut over vanilla in the human study.** DiMOO-Shortcut emulates the vanilla model in perceptual quality in most cases.

$(15 - 1) \times 2 = 28$ training samples, for a total of 1.4M. We train MaskGIT-Shortcut for 5 hours using 4 H200 GPUs.

We evaluate the generation quality on ImageNet-512 by FID (Heusel et al., 2017). The performance of MaskGIT with and without shortcut under different configurations is shown in Tab. 1 and Fig. 5. We can see MaskGIT-Shortcut can consistently generate better images at a faster speed, even surpassing the vanilla’s optimal performance. This phenomenon is somewhat strange. Intuitively, the upper bound of MaskGIT-Shortcut performance should have been the vanilla MaskGIT with the same number of steps. However, in our experiments, the MaskGIT-Shortcut with 32 steps and budget 8/9/12 all surpass vanilla MaskGIT with 32 steps. We provide a possible explanation as follows. It has been observed that increasing the number of steps may degrade the performance (Chang et al., 2022). For example, Besnier & Chen (2023) reports the optimal number of steps as 15. That is to say, the feature trajectories under 15 steps are better than those under 32 steps. Our MaskGIT-Shortcut is trained on feature trajectories generated by MaskGIT with 15 steps. If well-trained, it will evolve along this golden trajectory that more accurately leads to the target data distribution than the 32-step trajectory, thus achieving lower FID. Besides, when compared with vanilla MaskGIT with 15 steps, MaskGIT-Shortcut with 32 steps takes the same trajectory but moves with a finer step size, thus also able to achieve better performance. This hypothesis highlights that as MIGM-Shortcut learns the latent dynamics, it may improve not only efficiency but also performance.

4.2. Text-to-Image Generation using Lumina-DiMOO

Setup. The shortcut model applied to Lumina-DiMOO is termed DiMOO-Shortcut. It has 220M parameters, only 1/37 of the original Lumina-DiMOO. The latency of one invocation is around 1/30 of the base model. We use prompts from Chen et al. (2025b) to prompt Lumina-DiMOO to generate 2000 images of resolution 1024×1024 in 64 steps. Each image corresponds to $(64 - 1) \times 2 = 126$ training samples, totaling 252K. We train DiMOO-Shortcut for 12

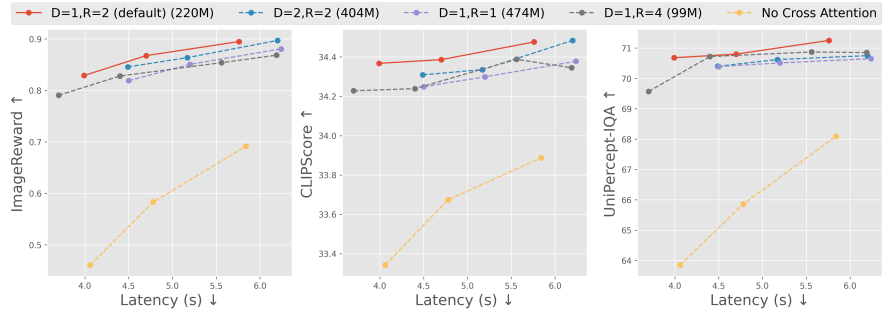


Figure 9. **Quality-speed tradeoff of different model designs of MIGM-Shortcut.** The solid red line denotes the default, and the dash lines denote ablated variants. All models infer with 64 steps and budget 14/11/9, and the lighter variant $D = 1, R = 4$ has an extra budget 16.

hours using 4 H200 GPUs, which is also a modest cost.

Evaluation protocol. Following common practice (Zheng et al., 2025b; Liu et al., 2025c; Feng et al., 2025), we evaluate the quality of generated images by ImageReward (Xu et al., 2023) and CLIPScore (Hessel et al., 2021). We also report UniPercept-IQA (Cao et al., 2025), a recent advanced metric based on multi-modal large language models. The prompts are from Hu et al. (2024), and the resolution is 1024×1024 .

Compared methods. We compare DiMOO-Shortcut with various acceleration methods. The most straightforward baseline is reducing the steps of Lumina-DiMOO. It also has a unique training-free acceleration technique called ML-Cache, which reports $2\times$ speedup. Other compared methods include ReCAP (Liu et al., 2025d), dLLM-Cache (Liu et al., 2025e), and TaylorSeer (Liu et al., 2025c). They are all training-free but not officially implemented on Lumina-DiMOO, so we adapt them to Lumina-DiMOO. ReCAP (Liu et al., 2025d) is a general acceleration method for MIGMs. dLLM-Cache (Liu et al., 2025e) is designed for diffusion language models, but the open-sourced code repository also implements it on the text-to-image task using MMaDA (Yang et al., 2025), which shares a similar architecture with Lumina-DiMOO. TaylorSeer (Liu et al., 2025c) is a cutting-edge method for continuous diffusion, forecasting the next feature from previous features. Besides these generally applied plug-and-play acceleration techniques, we also include a one-step MIGM Di[M]O for comparison, which is distilled from Meissonic (Bai et al., 2025) and achieves extremely fast speed.

Accelerating effects. All the methods except Di[M]O have several configurable hyper-parameters to allow for a flexible quality-speed tradeoff. We carefully tune them and report the Pareto-optimal configurations of each method. For each of these methods, we report two configurations: one that barely maintains quality while maximizing speed, and one that becomes a little faster but considerably compromises the

quality. The acceleration is with respect to Lumina-DiMOO using 64 steps. Tab. 2 lists the results, and Fig. 6 provides a more clear visualization. We can see that all three configurations of DiMOO-Shortcut approach the performance of the vanilla, while reaching $4.0 \sim 5.8$ acceleration rate. Notably, under budget $B = 14$, DiMOO-Shortcut achieves the highest ImageReward and UniPercept-IQA, and the second highest CLIPScore, with a high acceleration rate of 4. Although ReCAP can achieve a slightly higher CLIPScore, its two other metrics are very low, and the acceleration rate is also lower. Some qualitative examples are shown in Fig. 7, also supporting the superiority of DiMOO-Shortcut. For more examples please refer to Appendix D. To further validate the maintained perceptual quality of DiMOO-Shortcut results, we conduct a human study on the Rapidata platform³, asking humans to compare the quality of images before and after acceleration by DiMOO-Shortcut. Fig. 8 shows the win rates of DiMOO-Shortcut. In nearly half the cases, DiMOO-Shortcut with $B = 14$ and $4.0\times$ speedup is considered better. Even with $B = 9$ and $5.8\times$ speedup, the win rate still approaches 40%. These results demonstrate that DiMOO-Shortcut can indeed largely accelerate generation with minimal loss of quality.

It is noteworthy that although the one-step model Di[M]O is extremely fast, the image quality is unacceptable in many cases. This is due to the multi-modality problem (Gu et al., 2018). The MIGM can only model the marginal distribution of each token instead of the joint distribution of multiple tokens. This will cause severe performance degradation if the model tries to unmask too many tokens in a single step. Fig. 10 presents some examples. In the first row, when prompted to generate a single object, Di[M]O generates duplication; in the second row, it generates the same parts of an object in different locations, causing artifacts. Therefore, currently reducing the number of generation steps for MIGMs is particularly difficult, while MIGM-Shortcut can reduce the number of costly full steps, behaving like pseudo few-step generation.

4.3. Ablation Study

We ablate the model design on DiMOO-Shortcut to validate our two assumptions discussed in Sec. 1. All variants are trained for over 12 hours using 4 H200 GPUs. More details are in Appendix E.

Importance of incorporating sampling information.

The feature dynamics are controlled by the sampling, hence it is a must to incorporate this information to predict features. We implement this via the cross-attention module. To investigate its influence, we replace the cross attention with self attention so that the model cannot attend to sampled tokens. As Fig. 9 shows, removing the cross attention

³<https://www.rapidata.ai/>. More details are in Appendix C.

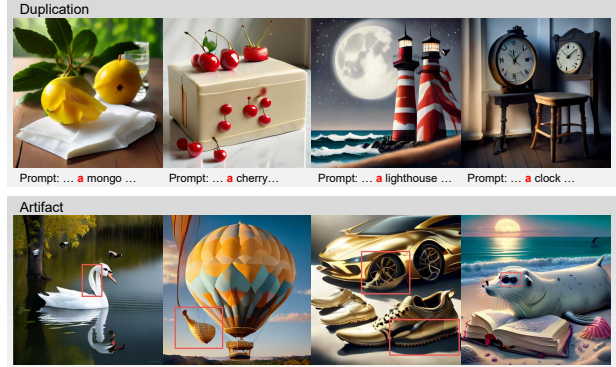


Figure 10. Examples of the multi-modality problem in Di[M]O. In a single step, the MIGM cannot jointly model the distribution of multiple tokens, causing duplication or even artifacts.



Figure 11. Comparison of DiMOO-Shortcut with and without incorporating sampling information. The right two images are over-smoothed.

drastically degrades the performance. Fig. 11 presents two examples. The shortcut model without cross attention tends to output over-smoothed images, as it is forced to predict the expectation over all possible sampling results.

Model complexity. The complexity of the shortcut model should strike a balance. Too low complexity cannot accurately model feature dynamics, like existing caching-based methods, while too high complexity wastes computation, like the base model itself. To investigate this, we modify the model size by altering the bottleneck ratio R and the number of cross attention and self attention layers D (the setting adopted in the experiments in Sec. 4.1 and 4.2 is $R = 2, D = 1$). The variants' performance is shown in Fig. 9, with the configurations and parameter numbers indicated in the legend. Although the heavier variants sometimes surpass the default under the same budget, the performance gain cannot compensate for the increased latency. On the other hand, making the model lighter compromises performance, which cannot be remedied by increasing the budget. Therefore, among these variants, our default setting is still Pareto optimal, at a sweet spot of model complexity.

5. Conclusion

This paper presents MIGM-Shortcut, which achieves remarkable acceleration with minimal performance drop. We identify that the sampling process of MIGMs wastes much information in the continuous features, hence leveraging this information may reduce the computational complexity.

For existing related methods that use previous features to approximate future ones, we point out that they suffer from limited expressivity and the fatal neglect of sampling information. Accordingly, we propose to learn a lightweight model that incorporates both previous features and sampled tokens to learn the dynamics of latent feature evolution. The learned model takes a shortcut that skips the heavy base model to improve efficiency. Experiments on MaskGIT and Lumina-DiMOO demonstrate the effectiveness and rationale of MIGM-Shortcut. We hope this paper could provide more insights into the computation paradigm of MIGMs, especially about its inherent redundancy.

Acknowledgements

This work is supported by Shanghai Artificial Intelligence Laboratory.

Impact Statement

This paper presents work whose goal is to advance the field of Machine Learning. There are many potential societal consequences of our work, none which we feel must be specifically highlighted here.

References

- Austin, J., Johnson, D. D., Ho, J., Tarlow, D., and van den Berg, R. Structured denoising diffusion models in discrete state-spaces. In *Advances in Neural Information Processing Systems*, volume 34, pp. 17981–17993. Curran Associates, Inc., 2021.
- Bai, J., Ye, T., Chow, W., Song, E., Chen, Q.-G., Li, X., Dong, Z., Zhu, L., and Yan, S. Meissonic: Revitalizing masked generative transformers for efficient high-resolution text-to-image synthesis. In *The Thirteenth International Conference on Learning Representations*, 2025.
- Besnier, V. and Chen, M. A pytorch reproduction of masked generative image transformer. *arXiv preprint arXiv:2310.14400*, 2023.
- Besnier, V., Chen, M., Hurych, D., Valle, E., and Cord, M. Halton scheduler for masked generative image transformer. In *The Thirteenth International Conference on Learning Representations*, 2025.
- Cao, S., Li, J., Li, X., Pu, Y., Zhu, K., Gao, Y., Luo, S., Xin, Y., Qin, Q., Zhou, Y., et al. UniPercept: Towards unified perceptual-level image understanding across aesthetics, quality, structure, and texture. *arXiv preprint arXiv:2512.21675*, 2025.
- Chang, H., Zhang, H., Jiang, L., Liu, C., and Freeman, W. T. MaskGIT: Masked generative image transformer. In *Proceedings of the IEEE/CVF Conference on Computer Vision and Pattern Recognition (CVPR)*, pp. 11315–11325, June 2022.
- Chang, H., Zhang, H., Barber, J., Maschinot, A., Lezama, J., Jiang, L., Yang, M.-H., Murphy, K. P., Freeman, W. T., Rubinstein, M., Li, Y., and Krishnan, D. Muse: Text-to-image generation via masked generative transformers. In *Proceedings of the 40th International Conference on Machine Learning*, volume 202, pp. 4055–4075. PMLR, 23–29 Jul 2023.
- Chen, G., Zhao, X., Zhou, Y., Qu, X., Chen, T., and Cheng, Y. Towards stabilized and efficient diffusion transformers through long-skip-connections with spectral constraints. In *Proceedings of the IEEE/CVF International Conference on Computer Vision (ICCV)*, pp. 17708–17718, October 2025a.
- Chen, J., Xu, Z., Pan, X., Hu, Y., Qin, C., Goldstein, T., Huang, L., Zhou, T., Xie, S., Savarese, S., et al. BLIP3-o: A family of fully open unified multimodal models-architecture, training and dataset. *arXiv preprint arXiv:2505.09568*, 2025b.
- Chen, P., Shen, M., Ye, P., Cao, J., Tu, C., Bouganis, C.-S., Zhao, Y., and Chen, T. Δ -DiT: A training-free acceleration method tailored for diffusion transformers. *arXiv preprint arXiv:2406.01125*, 2024.
- Deng, J., Dong, W., Socher, R., Li, L.-J., Li, K., and Fei-Fei, L. ImageNet: A large-scale hierarchical image database. In *2009 IEEE Conference on Computer Vision and Pattern Recognition*, pp. 248–255, 2009.
- Devlin, J., Chang, M.-W., Lee, K., and Toutanova, K. BERT: Pre-training of deep bidirectional transformers for language understanding. In *Proceedings of the 2019 Conference of the North American Chapter of the Association for Computational Linguistics: Human Language Technologies, Volume 1 (Long and Short Papers)*, pp. 4171–4186. Association for Computational Linguistics, June 2019.
- Esser, P., Rombach, R., and Ommer, B. Taming transformers for high-resolution image synthesis. In *Proceedings of the IEEE/CVF Conference on Computer Vision and Pattern Recognition (CVPR)*, pp. 12873–12883, June 2021.
- Fang, G., Ma, X., and Wang, X. Structural pruning for diffusion models. In *Advances in Neural Information Processing Systems*, volume 36, pp. 16716–16728. Curran Associates, Inc., 2023.
- Feng, L., Zheng, S., Liu, J., Lin, Y., Zhou, Q., Cai, P., Wang, X., Chen, J., Zou, C., Ma, Y., et al. HiCache:

- Training-free acceleration of diffusion models via Hermite polynomial-based feature caching. *arXiv preprint arXiv:2508.16984*, 2025.
- Frans, K., Hafner, D., Levine, S., and Abbeel, P. One step diffusion via shortcut models. In *The Thirteenth International Conference on Learning Representations*, 2025.
- Geng, Z., Deng, M., Bai, X., Kolter, J. Z., and He, K. Mean flows for one-step generative modeling. In *Advances in Neural Information Processing Systems*, 2025.
- Gu, J., Bradbury, J., Xiong, C., Li, V. O., and Socher, R. Non-autoregressive neural machine translation. In *International Conference on Learning Representations*, 2018.
- He, K., Zhang, X., Ren, S., and Sun, J. Deep residual learning for image recognition. In *Proceedings of the IEEE Conference on Computer Vision and Pattern Recognition (CVPR)*, June 2016.
- He, K., Chen, X., Xie, S., Li, Y., Dollár, P., and Girshick, R. Masked autoencoders are scalable vision learners. In *Proceedings of the IEEE/CVF Conference on Computer Vision and Pattern Recognition (CVPR)*, pp. 16000–16009, June 2022.
- Hessel, J., Holtzman, A., Forbes, M., Le Bras, R., and Choi, Y. CLIPScore: A reference-free evaluation metric for image captioning. In *Proceedings of the 2021 Conference on Empirical Methods in Natural Language Processing*, pp. 7514–7528. Association for Computational Linguistics, November 2021.
- Heusel, M., Ramsauer, H., Unterthiner, T., Nessler, B., and Hochreiter, S. GANs trained by a two time-scale update rule converge to a local nash equilibrium. In *Advances in Neural Information Processing Systems*, volume 30. Curran Associates, Inc., 2017.
- Ho, J., Jain, A., and Abbeel, P. Denoising diffusion probabilistic models. In *Advances in Neural Information Processing Systems*, volume 33, pp. 6840–6851. Curran Associates, Inc., 2020.
- Hu, X., Wang, R., Fang, Y., Fu, B., Cheng, P., and Yu, G. ELLA: Equip diffusion models with LLM for enhanced semantic alignment. *arXiv preprint arXiv:2403.05135*, 2024.
- Huang, X., Li, Z., He, G., Zhou, M., and Shechtman, E. Self forcing: Bridging the train-test gap in autoregressive video diffusion. In *Advances in Neural Information Processing Systems*, 2025.
- Isola, P., Zhu, J.-Y., Zhou, T., and Efros, A. A. Image-to-image translation with conditional adversarial networks. In *Proceedings of the IEEE Conference on Computer Vision and Pattern Recognition (CVPR)*, July 2017.
- Kidger, P., Morrill, J., Foster, J., and Lyons, T. Neural controlled differential equations for irregular time series. In *Advances in Neural Information Processing Systems*, volume 33, pp. 6696–6707. Curran Associates, Inc., 2020.
- Kim, S. H., Hong, S., Jung, H., Park, Y., and Yun, S.-Y. KCLASS: KL-guided fast inference in masked diffusion models. In *Advances in Neural Information Processing Systems*, 2025.
- Li, T., Chang, H., Mishra, S., Zhang, H., Katabi, D., and Krishnan, D. MAGE: Masked generative encoder to unify representation learning and image synthesis. In *Proceedings of the IEEE/CVF Conference on Computer Vision and Pattern Recognition (CVPR)*, pp. 2142–2152, June 2023.
- Liu, F., Zhang, S., Wang, X., Wei, Y., Qiu, H., Zhao, Y., Zhang, Y., Ye, Q., and Wan, F. Timestep embedding tells: It’s time to cache for video diffusion model. In *Proceedings of the IEEE/CVF Conference on Computer Vision and Pattern Recognition (CVPR)*, pp. 7353–7363, June 2025a.
- Liu, J., Wang, X., Lin, Y., Wang, Z., Wang, P., Cai, P., Zhou, Q., Yan, Z., Yan, Z., Shi, Z., et al. A survey on cache methods in diffusion models: Toward efficient multi-modal generation. *arXiv preprint arXiv:2510.19755*, 2025b.
- Liu, J., Zou, C., Lyu, Y., Chen, J., and Zhang, L. From reusing to forecasting: Accelerating diffusion models with taylorseers. In *Proceedings of the IEEE/CVF International Conference on Computer Vision (ICCV)*, pp. 15853–15863, October 2025c.
- Liu, X., Liu, A., den Broeck, G. V., and Liang, Y. Plug-and-play context feature reuse for efficient masked generation. In *Advances in Neural Information Processing Systems*, 2025d.
- Liu, Z., Yang, Y., Zhang, Y., Chen, J., Zou, C., Wei, Q., Wang, S., and Zhang, L. dLLM-Cache: Accelerating diffusion large language models with adaptive caching. *arXiv preprint arXiv:2506.06295*, 2025e.
- Lu, C., Zhou, Y., Bao, F., Chen, J., LI, C., and Zhu, J. DPM-Solver: A fast ODE solver for diffusion probabilistic model sampling in around 10 steps. In *Advances in Neural Information Processing Systems*, volume 35, pp. 5775–5787. Curran Associates, Inc., 2022.
- Ma, X., Fang, G., and Wang, X. DeepCache: Accelerating diffusion models for free. In *Proceedings of the IEEE/CVF Conference on Computer Vision and Pattern Recognition (CVPR)*, pp. 15762–15772, June 2024.

- Ni, Z., Wang, Y., Zhou, R., Guo, J., Hu, J., Liu, Z., Song, S., Yao, Y., and Huang, G. Revisiting non-autoregressive transformers for efficient image synthesis. In *Proceedings of the IEEE/CVF Conference on Computer Vision and Pattern Recognition (CVPR)*, pp. 7007–7016, June 2024a.
- Ni, Z., Wang, Y., Zhou, R., Han, Y., Guo, J., Liu, Z., Yao, Y., and Huang, G. ENAT: Rethinking spatial-temporal interactions in token-based image synthesis. In *Advances in Neural Information Processing Systems*, volume 37, pp. 90431–90455. Curran Associates, Inc., 2024b.
- Parmar, N., Vaswani, A., Uszkoreit, J., Kaiser, L., Shazeer, N., Ku, A., and Tran, D. Image transformer. In *Proceedings of the 35th International Conference on Machine Learning*, volume 80, pp. 4055–4064. PMLR, 10–15 Jul 2018.
- Peebles, W. and Xie, S. Scalable diffusion models with transformers. In *Proceedings of the IEEE/CVF International Conference on Computer Vision (ICCV)*, pp. 4195–4205, October 2023.
- Qiu, J., Wang, S., Lu, J., Liu, L., Jiang, H., Zhu, X., and Hao, Y. Accelerating diffusion transformer via error-optimized cache. In *Proceedings of the 33rd ACM International Conference on Multimedia*, MM ’25, pp. 9588–9597. Association for Computing Machinery, 2025.
- Ramesh, A., Pavlov, M., Goh, G., Gray, S., Voss, C., Radford, A., Chen, M., and Sutskever, I. Zero-shot text-to-image generation. In *Proceedings of the 38th International Conference on Machine Learning*, volume 139, pp. 8821–8831. PMLR, 18–24 Jul 2021.
- Romero, A., Ballas, N., Kahou, S. E., Chassang, A., Gatta, C., and Bengio, Y. FitNets: Hints for thin deep nets. In *International Conference on Learning Representations*, 2015.
- Salimans, T. and Ho, J. Progressive distillation for fast sampling of diffusion models. In *International Conference on Learning Representations*, 2022.
- Selvaraju, P., Ding, T., Chen, T., Zharkov, I., and Liang, L. FORA: Fast-forward caching in diffusion transformer acceleration. *arXiv preprint arXiv:2407.01425*, 2024.
- Shang, Y., Yuan, Z., Xie, B., Wu, B., and Yan, Y. Post-training quantization on diffusion models. In *Proceedings of the IEEE/CVF Conference on Computer Vision and Pattern Recognition (CVPR)*, pp. 1972–1981, June 2023.
- Shao, S., Zhou, Z., Ye, T., Bai, L., Xu, Z., and Xie, Z. Bag of design choices for inference of high-resolution masked generative transformer. *arXiv preprint arXiv:2411.10781*, 2024.
- Song, Y., Dhariwal, P., Chen, M., and Sutskever, I. Consistency models. In *Proceedings of the 40th International Conference on Machine Learning*, volume 202, pp. 32211–32252. PMLR, 23–29 Jul 2023.
- van den Oord, A., Kalchbrenner, N., and Kavukcuoglu, K. Pixel recurrent neural networks. In *Proceedings of The 33rd International Conference on Machine Learning*, volume 48, pp. 1747–1756. PMLR, 20–22 Jun 2016.
- van der Maaten, L. and Hinton, G. Visualizing data using t-SNE. *Journal of Machine Learning Research*, 9(86): 2579–2605, 2008.
- Vaswani, A., Shazeer, N., Parmar, N., Uszkoreit, J., Jones, L., Gomez, A. N., Kaiser, L. u., and Polosukhin, I. Attention is all you need. In *Advances in Neural Information Processing Systems*, volume 30. Curran Associates, Inc., 2017.
- Wimbauer, F., Wu, B., Schoenfeld, E., Dai, X., Hou, J., He, Z., Sanakoyeu, A., Zhang, P., Tsai, S., Kohler, J., Rupprecht, C., Cremers, D., Vajda, P., and Wang, J. Cache me if you can: Accelerating diffusion models through block caching. In *Proceedings of the IEEE/CVF Conference on Computer Vision and Pattern Recognition (CVPR)*, pp. 6211–6220, June 2024.
- Xie, Z., Zhang, Z., Cao, Y., Lin, Y., Bao, J., Yao, Z., Dai, Q., and Hu, H. SimMIM: A simple framework for masked image modeling. In *Proceedings of the IEEE/CVF Conference on Computer Vision and Pattern Recognition (CVPR)*, pp. 9653–9663, June 2022.
- Xie, Z., Zhang, Z., Cao, Y., Lin, Y., Wei, Y., Dai, Q., and Hu, H. On data scaling in masked image modeling. In *Proceedings of the IEEE/CVF Conference on Computer Vision and Pattern Recognition (CVPR)*, pp. 10365–10374, June 2023.
- Xin, Y., Qin, Q., Luo, S., Zhu, K., Yan, J., Tai, Y., Lei, J., Cao, Y., Wang, K., Wang, Y., et al. Lumina-DiMOO: An omni diffusion large language model for multimodal generation and understanding. *arXiv preprint arXiv:2510.06308*, 2025.
- Xu, J., Liu, X., Wu, Y., Tong, Y., Li, Q., Ding, M., Tang, J., and Dong, Y. ImageReward: Learning and evaluating human preferences for text-to-image generation. In *Advances in Neural Information Processing Systems*, volume 36, pp. 15903–15935. Curran Associates, Inc., 2023.
- Yan, F., Wei, Q., Tang, J., Li, J., Wang, Y., Hu, X., Li, H., and Zhang, L. LazyMAR: Accelerating masked autoregressive models via feature caching. In *Proceedings of the IEEE/CVF International Conference on Computer Vision (ICCV)*, pp. 15552–15561, October 2025.

- Yang, L., Tian, Y., Li, B., Zhang, X., Shen, K., Tong, Y., and Wang, M. MMaDA: Multimodal large diffusion language models. In *Advances in Neural Information Processing Systems*, 2025.
- Yin, T., Gharbi, M., Zhang, R., Shechtman, E., Durand, F., Freeman, W. T., and Park, T. One-step diffusion with distribution matching distillation. In *Proceedings of the IEEE/CVF Conference on Computer Vision and Pattern Recognition (CVPR)*, pp. 6613–6623, June 2024.
- You, Z., Ou, J., Zhang, X., Hu, J., Zhou, J., and Li, C. Effective and efficient masked image generation models. In *Proceedings of the 42nd International Conference on Machine Learning*, volume 267, pp. 72730–72746. PMLR, 13–19 Jul 2025.
- Zhang, L., Bao, C., and Ma, K. Self-distillation: Towards efficient and compact neural networks. *IEEE Transactions on Pattern Analysis and Machine Intelligence*, 44(8):4388–4403, 2022.
- Zheng, K., Chen, Y., Mao, H., Liu, M.-Y., Zhu, J., and Zhang, Q. Masked diffusion models are secretly time-agnostic masked models and exploit inaccurate categorical sampling. In *The Thirteenth International Conference on Learning Representations*, 2025a.
- Zheng, S., Feng, L., Wang, X., Zhou, Q., Cai, P., Zou, C., Liu, J., Lin, Y., Chen, J., Ma, Y., et al. Forecast then calibrate: Feature caching as ODE for efficient diffusion transformers. *arXiv preprint arXiv:2508.16211*, 2025b.
- Zhou, Z., Chen, D., Wang, C., Chen, C., and Lyu, S. Simple and fast distillation of diffusion models. In *Advances in Neural Information Processing Systems*, volume 37, pp. 40831–40860. Curran Associates, Inc., 2024.
- Zhu, Y., Wang, X., Lathuilière, S., and Kalogeiton, V. Di[M]O: Distilling masked diffusion models into one-step generator. In *Proceedings of the IEEE/CVF International Conference on Computer Vision (ICCV)*, pp. 18606–18618, October 2025.

A. Selecting which Layer’s Feature to Investigate

We inspect which layer’s feature is the most suitable for modeling by our MIGM-Shortcut. In order for MIGM-Shortcut to achieve higher acceleration rates, we hope to use the last layer’s feature. In order for the dynamics to be amenable to learning, we hope the cosine similarity between consecutive steps is the highest. Fig. 12 plots the similarity vs. the layer depth for an exemplary sample generated by Lumina-DiMOO. It turns out that the two conditions are achieved simultaneously: the last layer’s feature exhibit most stable dynamics. Therefore, we will use this feature as the modelling target of MIGM-Shortcut. We hypothesize that the reason may be that at the end of the neural network, as the feature directly dominates the generated distribution, it must be close to the training target, hence converging to a similar space across different steps.

B. More Exploration of Training Strategies

Beyond a simple MSE loss, we have also tried other strategies for training MIGM-Shortcut.

- **Adding distribution matching term to loss.** We add the KL divergence between the logits from the shortcut model’s features and the base model’s features:

$$D_{\text{KL}}(\text{softmax}(H(\hat{f})) \parallel \text{softmax}(H(f))),$$

where H is the frozen classification head of the base model.

- **Exposing shortcut model to its prediction.** At inference time, the input to the shortcut model may be its own feature prediction instead of the true features from the base model. This imposes a risk of exposure bias. Therefore, we propose that in training, let the shortcut model roll out for several steps, and then feed the resulting features into the model.

Although these methods seem to make sense, they do not bring notable benefits, as shown in Fig. 13. The reason may be that the dynamics are smooth enough and thus the target is easy enough to be learned by an MSE loss, which is in line with our core assumption.

C. Details of Human Study

We use the Rapidata⁴ platform to conduct pairwise human preference comparisons for evaluating image quality. Each trial presents various method outputs against vanilla output (A/B) under a fixed unified instruction:

Which image has better overall visual quality?

Annotators are vetted beforehand and participate on a voluntary basis.

For this study run, each acceleration method was evaluated on all paired datapoints, and each datapoint was annotated by three independent raters. We report, for each method M , the win rate against the vanilla defined as

$$\text{WinRate}(M \text{ vs. Vanilla}) = \frac{W_M}{W_M + W_{\text{Vanilla}}}, \tag{5}$$

where W_M and W_{Vanilla} denote the total numbers of pairwise wins for the method and the vanilla, respectively, aggregated over all collected comparisons.

D. More Visualization

Fig. 14-22 presents more examples of images generated by DiMOO-Shortcut and other compared methods, demonstrating that our method could consistently generate high-quality images with high speed.

E. Complete Results of Ablation Study

Tab. 3 lists the metric values of different variants of DiMOO-Shortcut. Among them, the default setting $N = 1, R = 2$ with cross attention achieves the optimal quality-speed tradeoff.

⁴<https://www.rapidata.ai/>

Table 3. Performance of different variants of DiMOO-Shortcut. N is the number of cross-attention and self-attention layers. R is the bottleneck ratio. “No cross attention” means replacing the cross-attention layer with a self-attention layer.

Method	Configuration	Latency (s)↓	ImageReward↑	CLIPScore↑	UniPercept-IQA↑
$N = 1, R = 2$ (default)	$B = 14$	5.76	0.90	34.48	71.25
	$B = 11$	4.70	0.87	34.39	70.80
	$B = 9$	3.99	0.83	34.37	70.68
$N = 2, R = 2$	$B = 14$	6.20	0.90	34.48	70.75
	$B = 11$	5.17	0.86	34.34	70.62
	$B = 9$	4.49	0.85	34.31	70.40
$N = 1, R = 1$	$B = 14$	6.24	0.88	34.38	70.65
	$B = 11$	5.20	0.85	34.30	70.51
	$B = 9$	4.50	0.82	34.25	70.39
$N = 1, R = 4$	$B = 16$	6.19	0.87	34.34	70.85
	$B = 14$	5.56	0.85	34.39	70.87
	$B = 11$	4.40	0.83	34.24	70.72
	$B = 9$	3.70	0.79	34.23	69.57
$N = 1, R = 2,$ no cross attention	$B = 14$	5.84	0.69	33.89	68.09
	$B = 11$	4.78	0.58	33.67	65.86
	$B = 9$	4.06	0.46	33.34	63.85

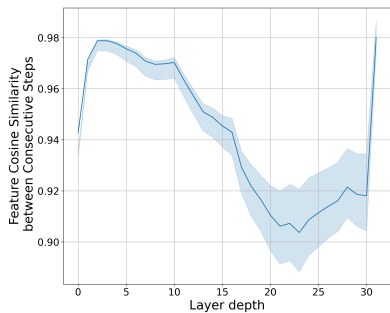


Figure 12. Feature cosine similarity between consecutive steps vs. layer depth. The line represents the average over all tokens, and the shade represents the range from 25% to 75% in all tokens.

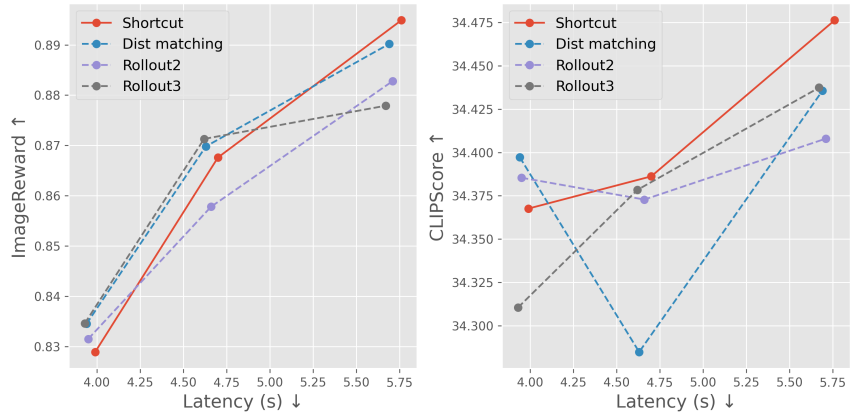


Figure 13. Comparison of different training strategies. “Dist matching” means adding a KL divergence term to the loss. “Rollout2/3” means rolling out 2/3 steps using the shortcut model in training.

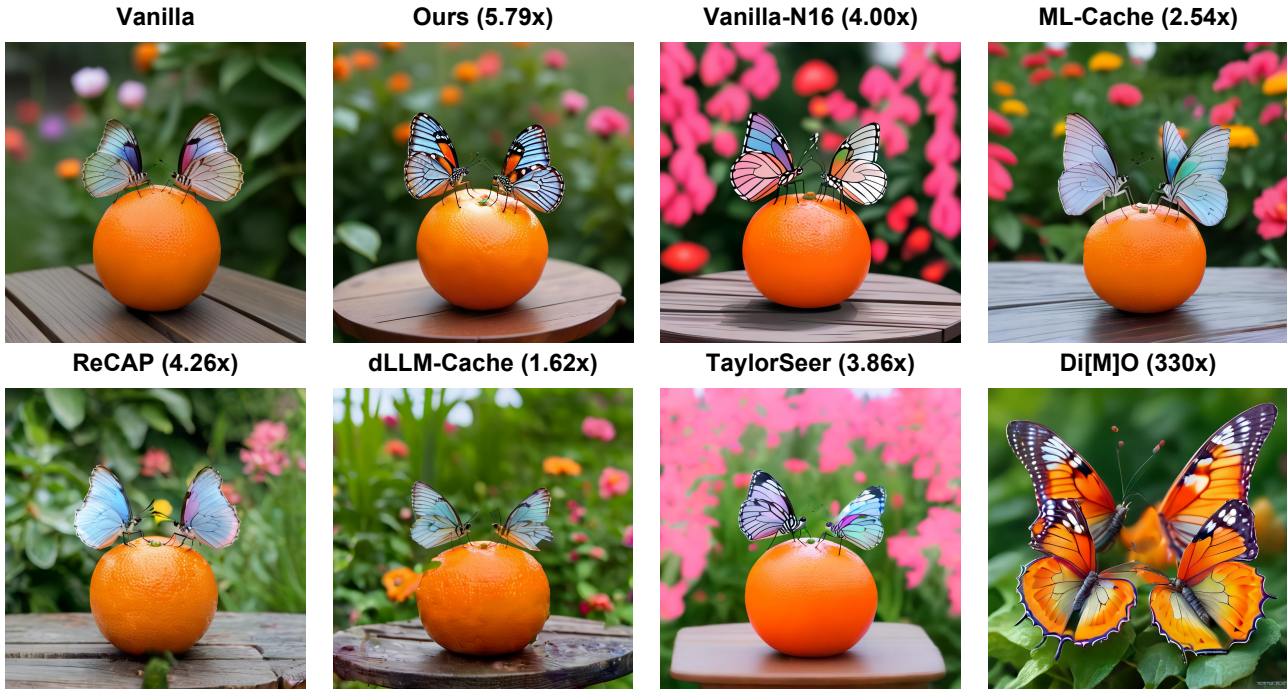


Figure 14. Prompt: Two multicolored butterflies with delicate, veined wings gently balance atop a vibrant, orange tangerine in a bustling garden. The tangerine, with its glossy, dimpled texture, is situated on a wooden table, contrasting with the greenery of the surrounding foliage and flowers. The butterflies, appearing nearly small in comparison, add a touch of grace to the scene, complementing the natural colors of the verdant backdrop.

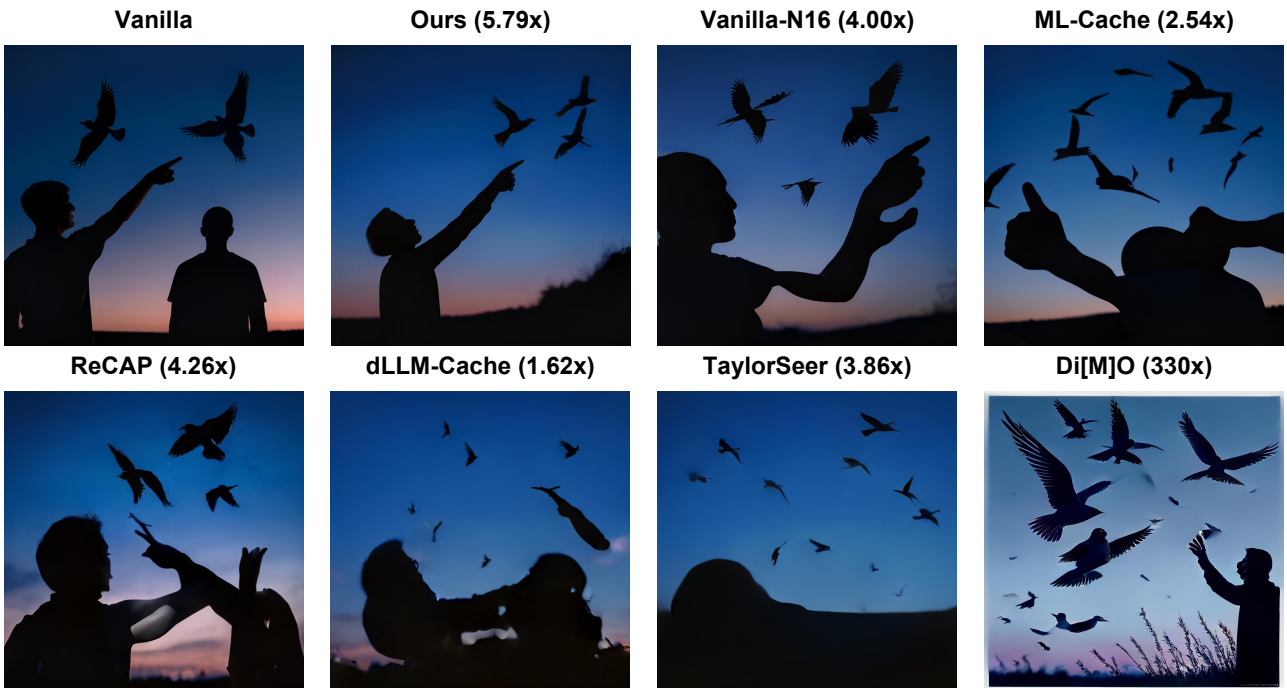


Figure 15. Prompt: During the twilight hour, an individual can be seen extending an arm towards the sky, pointing at a trio of wild birds gliding through the rich deep blue of the early evening sky. The birds' silhouettes contrast distinctly against the fading light, their wings spread wide as they soar. The person is silhouetted against the dusky sky, creating a peaceful scene of human connection with nature.



Figure 16. Prompt: In an elegantly simple room, two pairs of sandals—one blue and one red—sit tidily beneath a quaint, square wooden side table featuring a weathered finish that suggests a touch of rustic charm. The side table, which casts a soft shadow onto the textured salmon pink wall behind it, provides a harmonious balance to the vibrant footwear. The floor beneath the table is a polished light hardwood, reflecting a faint glow from the natural light entering the room.

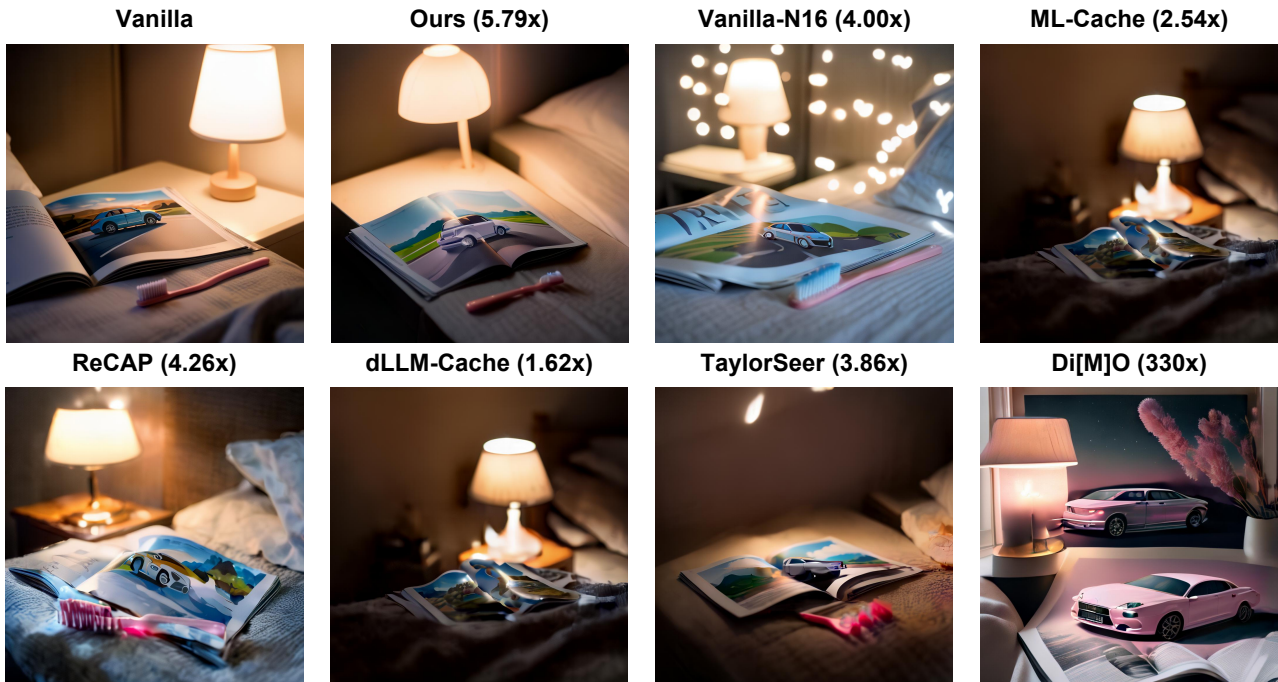


Figure 17. Prompt: Inside a dimly lit room, the low luminance emanates from a bedside lamp casting a soft glow upon the nightstand. There lies a travel magazine, its pages open to a vivid illustration of a car driving along a picturesque landscape. Positioned on the image is a light pink toothbrush, its bristles glistening in the ambient light. Beside the magazine, the textured fabric of the bedspread is just discernible, contributing to the composed and quiet scene.



Figure 18. Prompt: A delicate silver ring with a sleek band sits gracefully next to a large, dark leather wallet that seems to overflow with cards and receipts. Both items rest on a polished wooden bedside table, whose grain texture subtly complements the metallic luster of the ring. The wallet’s bulky appearance emphasizes the fine simplicity of the ring, highlighting the stark difference in their sizes and designs.



Figure 19. Prompt: A gleaming pair of golden cymbals lies in stark contrast to a collection of round, static bottles of toiletries arranged neatly on a shelf. The metallic sheen of the cymbals is emphasized by the surrounding muted tones of the shampoo and lotion containers. The bathroom shelf upon which they rest is made of polished oak, adding a warm touch to the setting.



Figure 20. Prompt: In an otherwise silent room, the melodic rhythm of a recorder being played gently reverberates throughout the space. A single lantern with a hexagonal frame and intricate metalwork sits nearby, emitting a soft, warm light that flickers subtly, illuminating the immediate vicinity. The walls, which are painted a muted cream color, catch the lantern’s glow, creating a cozy ambiance around the musician.



Figure 21. Prompt: A rustic, vintage wooden desk sitting in the corner of an antique store, its surface aged to a warm honey color. Upon the desk lies a silver flute, its polished surface gently reflecting the soft, golden light from the late afternoon sun streaming through a nearby window. Behind the flute, an array of eclectic cleaning products, from old-fashioned feather dusters to vintage glass bottles, is artfully arranged, adding to the charm of the setting. These items catch the sunlight in a way that casts an array of subtle shadows and highlights across the desk’s surface.

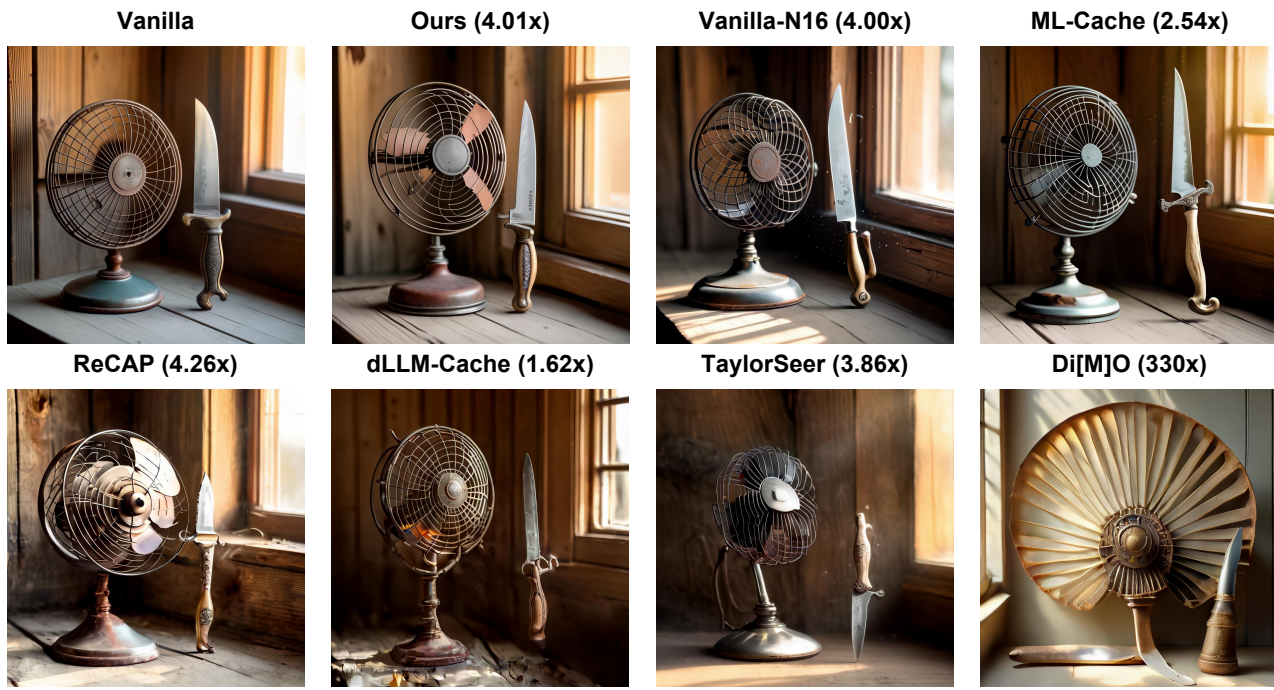


Figure 22. Prompt: An old fashioned, metallic fan with a rounded base and rusted blades stands next to an ornate, antique knife with a weathered bone handle. Both items are propped against a timeworn wooden wall that bears the marks of age and the warm, golden hue of the afternoon sunlight filtering through a nearby window. The dust particles in the air catch the light, highlighting the vintage aura of the scene.